




## Article

# Resistance of Thermally Aged DSS 2304 against Localized Corrosion Attack

Federica Zanotto <sup>1,2,\*</sup> , Vincenzo Grassi <sup>1</sup>, Andrea Balbo <sup>1</sup> , Cecilia Monticelli <sup>1</sup>  and Fabrizio Zucchi <sup>1</sup>

<sup>1</sup> “Aldo Daccò” Corrosion and Metallurgy Study Centre, University of Ferrara, Via G. Saragat 4A, 44122 Ferrara, Italy; vincenzo.grassi@unife.it (V.G.); andrea.balbo@unife.it (A.B.); mtc@unife.it (C.M.); zhff@unife.it (F.Z.)

<sup>2</sup> Terra & AcquaTech Laboratory, University of Ferrara, Via Saragat 1, 44122 Ferrara, Italy

\* Correspondence: zntfrc@unife.it; Tel.: +39-053-245-5195

Received: 31 October 2018; Accepted: 4 December 2018; Published: 5 December 2018



**Abstract:** In this paper, the effects of thermal aging in the 650–850 °C range on the localized corrosion behaviour of duplex stainless steel (DSS) 2304 was investigated. Pitting corrosion resistance was assessed by pitting potential ( $E_{\text{pitt}}$ ) and critical pitting temperature (CPT) determination, while the degree of sensitisation (DOS) to intergranular corrosion (IGC) was evaluated by double loop electrochemical potentiokinetic reactivation (DL-EPR). The susceptibility to stress corrosion cracking (SCC), evaluated in standard NACE TM-0177 solution at pH 2.7 and 25 °C, with the addition of  $\text{S}_2\text{O}_3^{2-}$  at  $10^{-3}$  M, resulted in general good agreement with pitting and IGC behaviour. In fact, as-received DSS 2304 aged for 5 min at 650 °C or 750 °C presented a high resistance to localized corrosion. The alloy corrosion behaviour was severely impaired with an aging time of 60 min at 650 °C and of 10 or 60 min at 750 °C, due to the precipitation of finely distributed  $\text{M}_{23}\text{C}_6$ -type chromium carbides at ferrite/austenite interphases, which determined the formation of chromium and molybdenum depleted areas. The behaviour of samples aged at 850 °C also depended on the aging time, but, at 60 min, the rediffusion of passivating elements produced a recovery of the alloy resistance to pitting, IGC and SCC.

**Keywords:** duplex stainless steel; pitting corrosion; intergranular corrosion; stress corrosion cracking; CPT; DL-EPR

## 1. Introduction

The significant mechanical and corrosion resistance performances of duplex stainless steels (DSS) are essentially related to their biphasic microstructure, characterized by an austenite/ferrite ratio close to 1 and by their chemical composition, which includes elements like chromium, molybdenum and nitrogen. However, these elements can cause the formation of deleterious secondary phases, such as  $\chi$  (chi) and  $\sigma$  (sigma) phases and chromium nitrides and/or carbides, if DSS are held, also for brief times, within the 550–950 °C temperature range [1,2]. The  $\sigma$  phase is an intermetallic compound, containing about 30% Cr, 4% Ni and 7% Mo, that nucleates preferentially at the ferrite and ferrite/austenite grain boundaries and then grows into the ferritic grains in DSS aged between 700 and 950 °C [3]. The  $\chi$ -phase, containing about 25% Cr, 3% Ni and 14% Mo, also forms within 700–900 °C, but in smaller amounts than  $\sigma$  [3]. Escriba et al. [4] observed that this phase was metastable in DSS 2205 grade and was consumed by the  $\sigma$ -phase precipitation. The precipitation of  $\text{Cr}_2\text{N}$  and  $\text{M}_{23}\text{C}_6$  type carbides is observed to occur simultaneously in the 550–1000 °C temperature range, but their formation is quicker at 700–900 °C [5]. Both the  $\chi$  and/or  $\sigma$  phase and the chromium nitride and/or carbide precipitation can determine a Cr-depletion in adjacent areas [5–9], with consequent impairment of

corrosion resistance. Moreover, Cr-depleted ferrite phase with high Ni content becomes unstable and eventually transforms into secondary austenite ( $\gamma_2$ ) [10–13], which is characterized by a significantly lower chromium concentration [5].

DSS 2304 (UNS 32304) was the first lean duplex stainless steel (LDSS) to be commercialized. It is a low-cost grade, due to Mo savings (Mo mass% around 0.3%), but also as a  $\sigma$ -free grade [14]. In fact, as already observed in a preceding study on LDSS 2101 [15], which also contains a Mo mass% around 0.3%, the kinetics of precipitation of  $\chi$  and  $\sigma$  phase mainly depend on Mo content [3]. In particular, in [15] it was observed that brief aging (from 5 to 60 min) between 650 and 850 °C on LDSS 2101 did not cause any  $\sigma$  phase formation, but the precipitation of chromium carbides and nitrides occurred at the ferrite ( $\alpha$ ) and austenite ( $\gamma$ ) grain boundaries or phase interfaces [16,17]. These precipitates were found to adversely affect the localized corrosion resistance of LDSS [12,15–19].

Few studies in the literature deal with the corrosion resistance of DSS 2304 after microstructural modifications. Some concern the influence of welding conditions [20–22], while others the effect of thermal aging on DSS 2304 corrosion behaviour [23–25]. Thus, a wider characterization of pitting and intergranular corrosion behaviour of this grade after thermal aging within a temperature range in which deleterious secondary phases can form is evidently an interesting topic. Moreover, the susceptibility to stress corrosion cracking (SCC) in critical environments, such as in media containing chlorides and hydrogen sulphide ( $H_2S$ ) as encountered by components of oil and gas extraction equipment, can be correlated to pitting and intergranular corrosion (IGC) resistance, thus giving information about the microstructural modifications which can cause early failures in field conditions.

With this aim, the pitting corrosion resistance of the alloy was evaluated by both anodic polarization curves recording in 1 M NaCl solution at 20 °C and critical pitting temperature (CPT) measurements in 0.1 M NaCl solution. The IGC susceptibility was studied by double loop electrochemical potentiokinetic reactivation (DL-EPR) technique carried out in 33%  $H_2SO_4$  solution with different amounts of HCl as depassivator. These electrochemical tests were performed under conditions specifically chosen to differentiate the response of the material after different thermal treatments in the 650–850 °C range, in order to evidence any corrosion resistance weakening. The SCC susceptibility of DSS 2304 was evaluated in standard NACE TM-0177 solution at pH 2.7 and 25 °C, in the presence of  $S_2O_3^{2-}$  at  $10^{-3}$  M, by slow strain rate tests (SSRT). The use of  $S_2O_3^{2-}$  ions in replacement of  $H_2S$  was discussed in our preceding papers [26–28]. Depending on the alloy potential and solution pH,  $S_2O_3^{2-}$  allows the assessment of the influence of  $H_2S$  on SCC resistance under health-safe testing conditions and at lower costs of experimental setup [29]. Finally, the correlation between the microstructural modifications produced by thermal aging and the electrochemical test and SSRT results was studied by observations under optical microscope (OM) and scanning electron microscope equipped with energy dispersion spectroscopy (SEM-EDS).

## 2. Materials and Methods

Annealed DSS 2304 alloy was provided by Outokumpu Company. The stainless steel chemical composition (wt%), evaluated by optical emission spectroscopy (OES), is shown in Table 1, where the alloy pitting resistance equivalent number ( $PRE_N$ ) is also reported.

**Table 1.** Chemical composition (wt%) of DSS 2304.

DSS	C	Mn	Cr	Ni	Mo	N	Si	Cu	V	S	P	Fe	$PRE_N$ *
DSS 2304	0.03	1.34	23.55	4.88	0.38	0.1	0.41	0.25	0.1	0.012	0.021	Bal.	26

\*  $PRE_N$  (pitting resistance equivalent number) = % Cr + 3.3% Mo + 16% N.

15 mm × 15 mm specimens were cut from a 1.5-mm thick steel sheet. The specimens were heat treated for 5, 10 and 60 min at 650, 750 and 850 °C and then cooled in air. The microstructures obtained were observed by Zeiss EVO MA15 SEM (Oberkochen, Germany), coupled to an Oxford Aztec EDS system (Oxford, United Kingdom).

### 2.1. Electrochemical Measurements

The electrochemical tests were performed on electrodes obtained by embedding DSS 2304 samples in an epoxy resin (exposed area about  $0.45 \text{ cm}^2$ ). The exposed surface was prepared with emery papers down to 2500 grit, polished by a diamond colloidal suspension (from 6 to  $1 \text{ }\mu\text{m}$ ), rinsed by deionized water and finally degreased by acetone.

The anodic polarization curves were recorded after 1 h immersion in 1 M NaCl solution at  $20 \text{ }^\circ\text{C}$ , starting from the open circuit potential ( $E_{\text{OCP}}$ ) and with a scan rate of  $0.1 \text{ mV/s}$ . The pitting potentials ( $E_{\text{pitt}}$ ) were determined from these curves and corresponded to the potential values at which the current density rapidly exceeded  $1 \text{ }\mu\text{A}\cdot\text{cm}^{-2}$ . Each  $E_{\text{pitt}}$  average value was obtained from triplicate tests.

CPT tests were carried out in 0.1 M NaCl solution by employing a potentiostatic polarisation method. The solution was thermostated at  $5 \text{ }^\circ\text{C}$  before the working electrode immersion. First, the electrode was cathodically polarized at  $-0.9 \text{ V}_{\text{SCE}}$  for 5 min in order to de-oxidize the surface and improve the test reproducibility [30]. Then, it was allowed to stabilize at  $E_{\text{OCP}}$  for 30 min. The CPT was determined by raising the electrolyte temperature by  $1 \text{ }^\circ\text{C/min}$  [31], at an applied potential of  $+0.75 \text{ V}_{\text{SCE}}$ . CPT was defined as the temperature at which the current exceeded  $100 \text{ }\mu\text{A}$  for at least 60 s. Each CPT average value was obtained from triplicate tests.

DL-EPR measurements were conducted in 33%  $\text{H}_2\text{SO}_4$  solution, at  $20 \text{ }^\circ\text{C}$ , with controlled addition of HCl (0.3, 0.45 and 0.6%) acting as depassivator [32]. The DSS samples were cathodically polarized at  $-0.6 \text{ V}_{\text{SCE}}$  for 3 min in order to improve the reproducibility. After 10 min stabilization under free corrosion conditions, the potential was cycled from  $E_{\text{OCP}}$  to  $+0.3 \text{ V}_{\text{SCE}}$  and then to  $E_{\text{OCP}}$  again, under a scan rate of  $2.5 \text{ mV/s}$ . According to the standard [33], the active dissolution in the depleted zones is proportional to the ratio  $I_r/I_a$ , where  $I_r$  is the peak current in the reverse scan (peak reactivation current) and  $I_a$  is the peak current in the anodic scan (peak activation current). The degree of susceptibility (DOS) to intergranular corrosion was estimated by the percent ratio  $(I_r/I_a) \times 100$  [34]. Below a  $(I_r/I_a) \times 100$  value of about 1, the corrosion rate calculated by weight loss is reported to be negligible, while above the ratio of 1 the change in the DOS is strongly reflected in the weight loss values [35]. Moreover, if  $(I_r/I_a) \times 100$  is higher than 5, the samples could fail the Streicher, Strauss and Huey tests [33]. After the tests, the IGC attack morphology was observed by both OM and SEM.

### 2.2. Slow Strain Rate Test in NACE TM-0177 Solution in the Presence of $\text{S}_2\text{O}_3^{2-}$

Slow strain rate tests were carried out on annealed and heat-treated samples in order to investigate their susceptibility to SCC. The SSRT were performed with a strain rate of  $10^{-6} \text{ s}^{-1}$  on samples (length 23 cm, gauge portion  $20 \times 5 \times 1.5 \text{ mm}^3$ ) prepared by EDM (electrical discharge machining). Heat treatments of 5, 10 and 60 min at  $650$ ,  $750 \text{ }^\circ\text{C}$  and  $850 \text{ }^\circ\text{C}$  were applied, followed by air cooling. Before the SSRT, the sample surfaces were polished with abrasive paper (down to 800 grit) and protected with an epoxy resin, with the exception of the gauge portion to be exposed to the aggressive environment. The test environment consisted of a de-aerated and thermostated ( $T = 25 \text{ }^\circ\text{C}$ ) solution containing 5% NaCl + 0.5%  $\text{CH}_3\text{COOH}$  (the basic standard solution NACE TM-0177 [36] but free of  $\text{H}_2\text{S}$ ) with the addition of  $10^{-3} \text{ M Na}_2\text{S}_2\text{O}_3$  (final pH = 2.7). Both open circuit potential values,  $E_{\text{OCP}}$ , and stress-strain curve were recorded during the tests. A saturated calomel electrode (SCE) was used as a reference electrode. Three tests were conducted for each adopted condition (annealed and heat treated samples, in solution and in air tests). The R ratios between the fracture strain percentage measured in the test solution and that in air were calculated for all heat treatment conditions in order to evaluate the corresponding susceptibility to SCC; in particular, R values  $\geq 0.8$  were considered as an indication of immunity to the SCC [37]. After the tests, the gauge portion of each sample was cut, polished and etched with Beraha's reagent to characterize the crack initiation and propagation morphology.

### 3. Results

#### 3.1. Microstructure

Figure 1 presents the microstructure of DSS 2304 aged for 5 to 60 min in the 650–850 °C range. Through observation with SEM in back-scattered electron (BSE), the austenitic phase (elongated in the rolling direction) was brighter than the ferritic phase, because of the higher nickel content of the former [16,38]. Due to the low molybdenum content of this alloy, no  $\chi$  and  $\sigma$  intermetallic phases were identified after the heat treatments adopted [17]. In the sample aged for 5 min at 650 °C (Figure 1b), no precipitates were observed at the grain boundaries. By prolonging the aging time to 60 min at 650 °C, very small black precipitates were detected at the  $\alpha/\gamma$  interphases (indicated by arrows, Figure 1c). After 10 and 60 min at 750 °C (Figure 1d,e), a more important precipitation of these intermetallic phases was observed and a brighter phase was observable between the precipitates and the ferrite matrix. This phase was likely the so-called secondary austenite ( $\gamma_2$ ) [17,38]. The thermal treatment performed for 60 min at 850 °C (Figure 1f) led to the formation of more voluminous black particles. In Figure 2 the results of SEM-EDS analysis, performed at several points along the yellow line, which passes through the black particles and the  $\gamma_2$  phase, are reported. The increase in wt% of chromium, molybdenum and carbon evidenced that these precipitates were essentially  $M_{23}C_6$ -type carbides, which are generally observed in DSS [5,39,40].

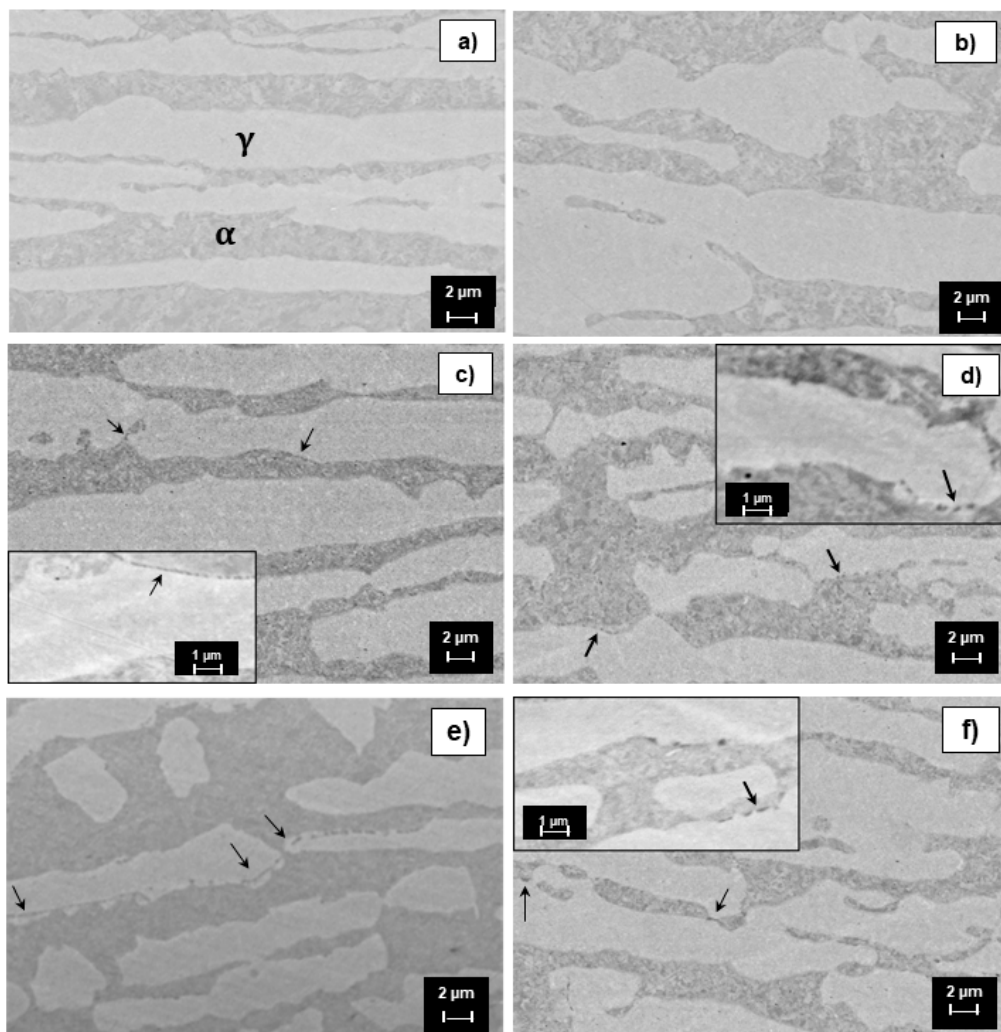


**Figure 1.** SEM-BSD micrographs of both duplex stainless steel (DSS) 2304 as-received (a) and aged for: 5 (b) and 60 min (c) at 650 °C, 10 (d) and 60 min (e) at 750 °C and 60 min at 850 °C (f).

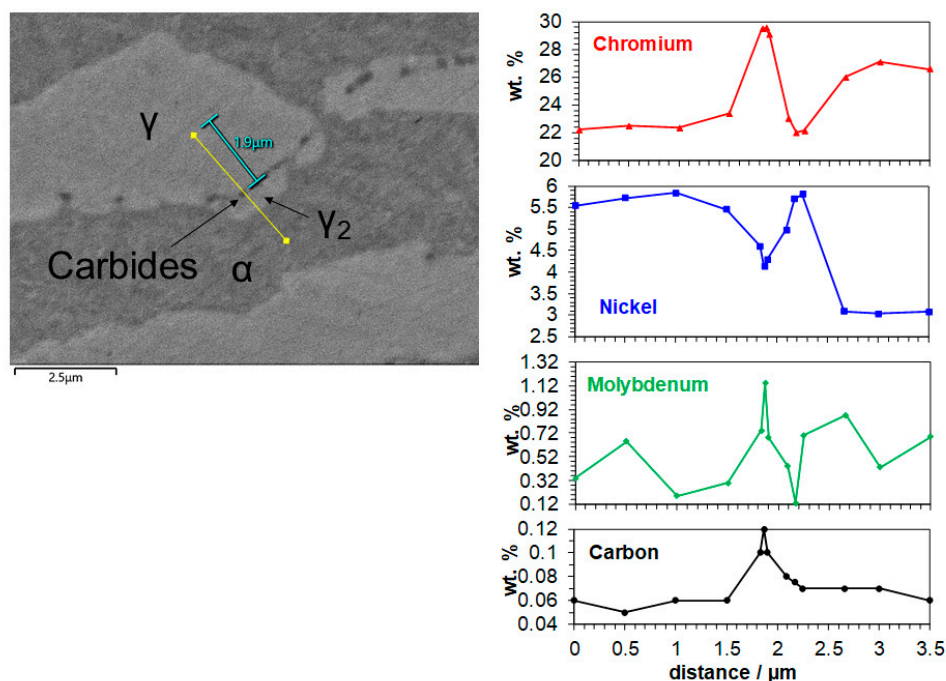


**Figure 2.** SEM-BSD image of DSS 2304 sample aged for 60 min at 750 °C. Quantitative profile line analysis of: chromium (red), nickel (blue), molybdenum (green) and carbon (black).

Figure 2 also clearly confirms the growth of  $\gamma_2$  due to chromium and molybdenum depletion and nickel enrichment in the original ferrite phase adjacent to the chromium carbides.

### 3.2. Pitting Potential Measurements

Table 2 collects the average  $E_{\text{pitt}}$  values obtained by the anodic polarization curves in 1 M NaCl solution at 20 °C on DSS 2304 electrodes aged at the three investigated temperatures.

**Table 2.** Average  $E_{\text{pitt}}$  values with standard deviation evaluated in 1 M NaCl solution at 20 °C on both as-received and aged DSS 2304 electrodes.

As-Received		$E_{\text{pitt}}$ (V <sub>SCE</sub> )							
		650 °C				750 °C		850 °C	
0 min	5 min	10 min	60 min	5 min	10 min	60 min	5 min	10 min	60 min
0.918 * ± 0.03	0.884 * ± 0.05	0.750 ± 0.08	0.481 ± 0.04	0.890 * ± 0.01	0.615 ± 0.01	0.336 ± 0.03	0.635 ± 0.06	0.640 ± 0.07	0.813 ± 0.04

\* Transpassive potential range.

As an example, in Figure 3 the anodic polarization curves recorded on samples, both as-received and aged at 750 °C for different times, are shown. For the as-received sample and for those aged for 5 min at 650 and 750 °C, a passive state was detected at  $E_{\text{OCP}}$  and at higher potentials up to about 0.8 V<sub>SCE</sub>, after which a transpassive behaviour occurred. After a 10-min treatment at these temperatures, the 2304 grade became moderately susceptible to pitting corrosion and  $E_{\text{pitt}}$  values of 0.750 (at 650 °C) and 0.615 (at 750 °C) V<sub>SCE</sub> were measured, but the passive current density ( $i_{\text{pass}}$ ) remained constant. After 60 min aging at 650 and 750 °C, a further drop in  $E_{\text{pitt}}$  was observed and values of 0.481 and 0.336 V<sub>SCE</sub> were obtained, respectively. A permanence of only 5 or 10 min at 850 °C produced a certain tendency to pitting corrosion at potentials higher than about 0.64 V<sub>SCE</sub>, but, in this case, a recovery of the corrosion resistance was observed by increasing the aging time to 60 min ( $E_{\text{pitt}}$  = 0.813 V<sub>SCE</sub>), most likely due to the replenishment of chromium by diffusion from the grain cores to the impoverished zones [11,15].

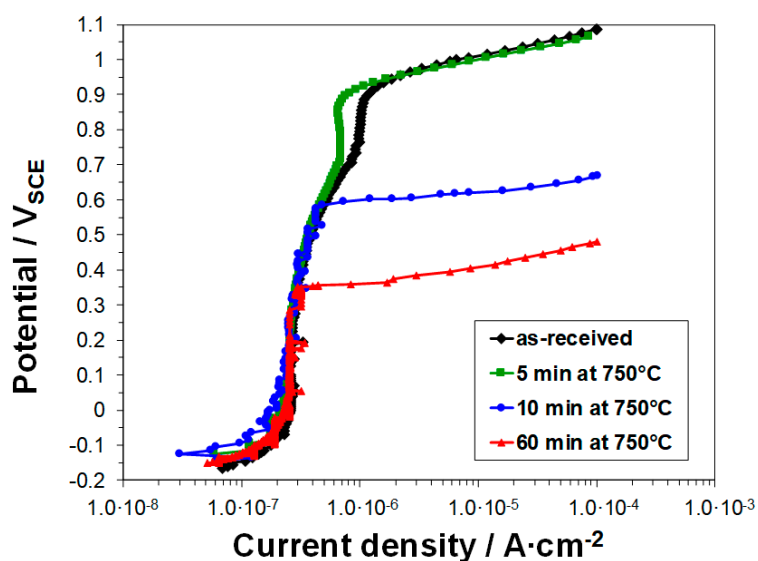


**Figure 3.** Anodic polarization curves recorded in 1 M NaCl solution at 20 °C on both as-received and aged DSS 2304.

### 3.3. CPT Test

Figure 4 shows the current density/temperature curves obtained for as-received and DSS 2304 electrodes aged at 750 °C during polarization at 0.75 V<sub>SCE</sub> in 0.1 M NaCl solution. In agreement with the potentiodynamic tests, the as-received and 5-min aged samples maintained very low current densities up to temperatures over 32 °C. Then, an abrupt current increase was observed and current values exceeded 100  $\mu\text{A}/\text{cm}^2$  at temperatures of  $35.3 \pm 1.1$  and  $35.2 \pm 1.3$  °C, respectively. A moderate decrease in CPT (about 6 °C) was detected for the sample aged at 750 °C for 10 min and, by extending the treatment time to 60 min, CPT decreased to  $21.2 \pm 0.6$  °C.

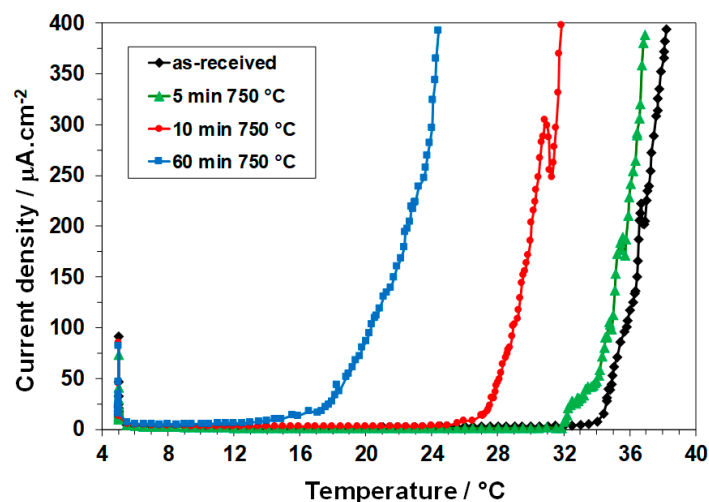


**Figure 4.** Current density vs. temperature curves obtained in 0.1 M NaCl solution on both as-received and aged DSS 2304.

Figure 5 reports the histogram that collects average CPT values in 0.1 M NaCl solution on DSS 2304 electrodes for all the tested aging conditions. The CPT values were in good agreement with the results of the potentiodynamic test. Both these techniques showed a significant reduction in pitting corrosion resistance after 60 min of aging at 650 °C, in comparison to that of as-received samples. At 750 °C, a 10-min aging was sufficient to have a relevant decrease in CPT and  $E_{\text{pitt}}$ , and a further

strong reduction was observed after 60 min. A 5- and 10-min aging at 850 °C also determined a significant tendency to pitting corrosion in 0.1 M NaCl solution. However, a recovery was detected after 60-min aging, with CPT and  $E_{\text{pitt}}$  only slightly lower than that obtained on as-received specimens.

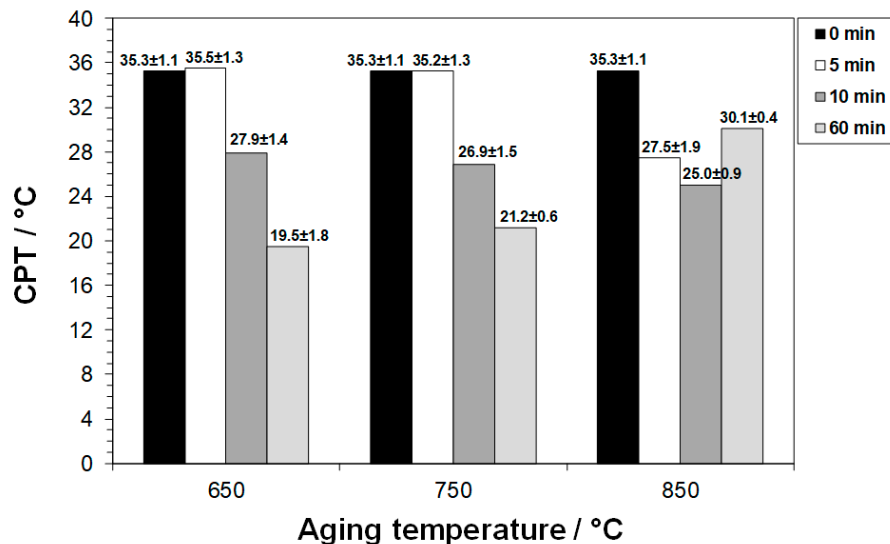


**Figure 5.** Average critical pitting temperature (CPT) values and standard deviations determined in 0.1 M NaCl solution for both as-received and aged DSS 2304.

Figure 6 shows a micrograph acquired on the surface of DSS 2304 electrode aged for 10 min at 750 °C after CPT test in 0.1 M NaCl solution. In agreement with the results of other authors [23,30], the localized corrosion attack appeared to start at the  $\gamma$  phase boundary, most likely in correspondence of Cr and Mo depleted areas around precipitates, then propagated in the ferrite phase, where relatively large pits formed.

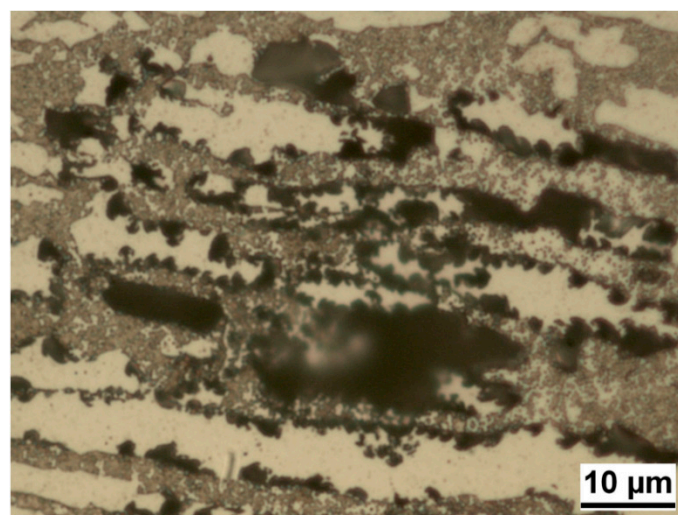


**Figure 6.** Micrograph of DSS 2304 electrode aged for 10 min at 750 °C after CPT test in 0.1 M NaCl solution (etching with Beraha's reagent).

### 3.4. DL-EPR Test

In order to determine the sensitivity of the alloys to IGC, the optimal concentration of the depassivator (HCl) to be added to the sulphuric acid solution was evaluated, prior to the extensive application of the DL-EPR technique. With this aim, preliminary tests were performed on both

as-received and 60-min aged DSS 2304, with HCl concentrations of 0.3, 0.45 and 0.6%. In Table 3, the Ir/Ia% ratios obtained under the different conditions are reported. A 0.3% HCl content was not enough to differentiate the DOS to IGC of the samples aged for 60 min at 750 and 850 °C. Moreover, with a HCl concentration of 0.6%, the as-received specimen showed Ir/Ia% values exceeding 1%, evidencing that a significant generalized corrosion had occurred, together with IGC [41]. In the presence of a 0.45% HCl, the as-received specimen maintained an Ir/Ia% value lower than 1%, while a good Ir/Ia% variation was detectable for the heat-treated samples, indicating that the attack selectively occurred at the grain boundary areas depleted in passivating elements.

**Table 3.** Ir/Ia% ratios and standard deviations in 33% H<sub>2</sub>SO<sub>4</sub> solution with different HCl concentrations, at 20 °C. Double loop electrochemical potentiokinetic reactivation (DL-EPR) tests performed on DSS 2304, both as-received and 60-min aged at 650, 750 and 850 °C.

HCl Concentration (%)	Ir/Ia%			
	As-Received	60 min 650 °C	60 min 750 °C	60 min 850 °C
0.3	0.02 ± 0.002	4.4 ± 0.05	0.2 ± 0.01	0.03 ± 0.003
0.45	0.08 ± 0.003	5.9 ± 0.07	1.4 ± 0.04	0.2 ± 0.02
0.6	1.7 ± 0.02	9.2 ± 0.11	5.2 ± 0.08	3.0 ± 0.05

Therefore, 0.45% HCl was chosen as the correct depassivator concentration to be used for all DL-EPR tests, and the DOS values obtained in 33% H<sub>2</sub>SO<sub>4</sub> + 0.45% HCl are presented as a histogram in Figure 7. Aging times of 5 and 10 min at 650 °C did not affect the resistance to IGC, whereas, 60-min aging at 650 °C determined a very high increase in Ir/Ia% parameter (significantly higher than that obtained with a treatment of 10 min). An aging of 10 min at 750 °C was sufficient to cause a high susceptibility to IGC (Ir/Ia% = 1.7%), maintained also on the sample aged for 60 min at the same temperature. The temperature of 850 °C did not determine susceptibility to IGC (Ir/Ia% < 1%), in spite of the formation of relatively large precipitates (Figure 1) [42].

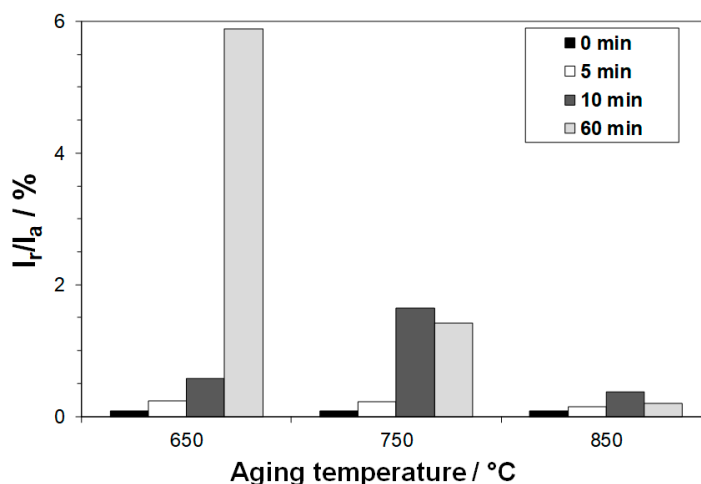


**Figure 7.** Ir/Ia% determined for as-received and aged DSS 2304, by DL-EPR tests in 33% H<sub>2</sub>SO<sub>4</sub> + 0.45% HCl solution, at 20 °C.

In Figure 8, the micrographs acquired by OM after DL-EPR tests on DSS 2304 electrodes heat treated for 60 min at different temperatures are reported. Confirmation of a marked IGC attack was detected in the 650 °C aged sample (DOS value of 5.9%). Instead, the IGC attack became less evident with the rise in aging temperature to 750 and 850 °C (DOS values of 1.4 and 0.2%, respectively).

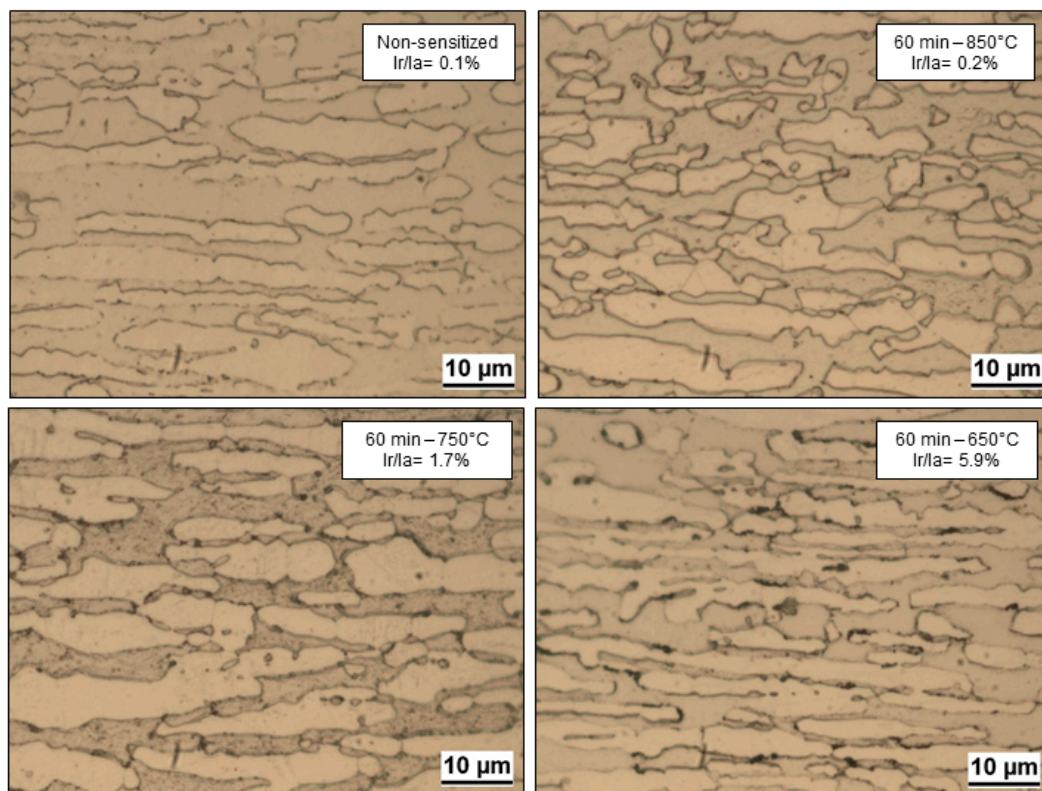


**Figure 8.** Optical microscope micrographs acquired on DSS 2304 electrodes after DL-EPR tests in 33% H<sub>2</sub>SO<sub>4</sub> solution, at 20 °C, with 0.45% HCl addition.

The DL-EPR results obtained for the 650 and 750 °C aged samples are in agreement with CPT values, suggesting that the thermal aging that were critical for pitting corrosion (i.e., 60 min at 650 °C and 10 and 60 min at 750 °C), also determined a very high susceptibility to IGC. The samples aged at 850 °C had very low DOS values even if a moderate decrease in pitting corrosion resistance was observed. Figure 9 reports some representative results of SEM-EDS analysis acquired after DL-EPR tests performed on DSS 2304 electrodes. The images of samples aged at 650 and 750 °C for 60 min show that the attack mainly occurred around the precipitates at the  $\alpha/\gamma$  interfaces, that is, on  $\gamma$  and likely on  $\gamma_2$  phases, due to passivating element depletion. The line elemental analysis performed by EDS across the precipitates revealed peaks related to chromium, molybdenum and carbon, confirming the presence of chromium and molybdenum carbides ( $M_{23}C_6$ -type precipitates [5]), while the small peak related to nitrogen suggests the likely concomitant formation of some nitrides [23,39].

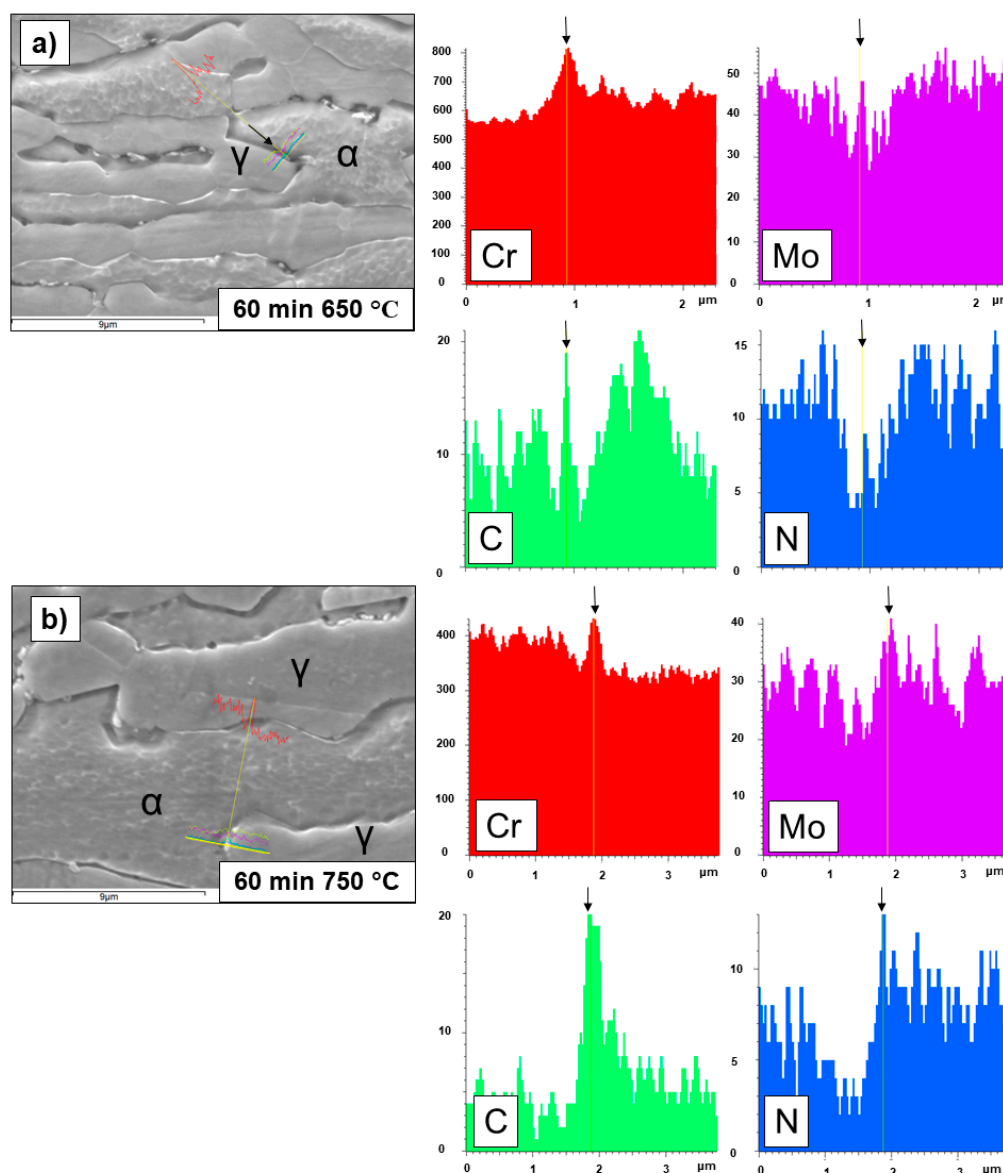


**Figure 9.** SEM-BSD micrographs of DSS 2304 aged for 60 min at 650 (a) and 750 °C (b), after DL-EPR test. Scanning electron microscope–energy dispersion spectroscopy (SEM-EDS) line profile analysis of: chromium (red), molybdenum (green), carbon (blue) and nitrogen (purple).

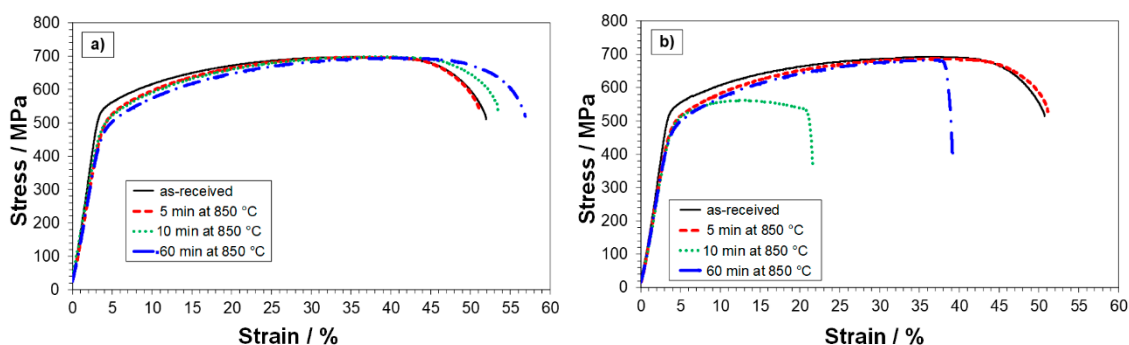
### 3.5. SSRT

Table 4 collects the average  $\epsilon_f\%$  values obtained with SSRT carried out in air at 25 °C and in NACE TM-0177 in the presence of  $10^{-3}$  M  $S_2O_3^{2-}$ , before and after thermal aging.

**Table 4.** Average values and standard deviations of  $\epsilon_f\%$  from slow strain rate tests (SSRT) performed in air at 25 °C and in NACE TM-0177 in the presence of  $10^{-3}$  M  $S_2O_3^{2-}$  on DSS 2304 as-received and thermally aged.

$\epsilon_f\%$	As Received	650 °C			750 °C			850 °C		
		5 min	10 min	60 min	5 min	10 min	60 min	5 min	10 min	60 min
Air at 25 °C	52 ± 1	52 ± 3	52 ± 2	50 ± 1	51 ± 2	52 ± 3	56 ± 2	51 ± 1	53 ± 2	57 ± 1
NACE TM-0177 with $10^{-3}$ M $S_2O_3^{2-}$	51 ± 2	51 ± 1	43 ± 1	18 ± 3	50 ± 3	22 ± 1	25 ± 3	51 ± 3	22 ± 2	39 ± 2

In air at 25 °C, only the samples aged for 60 min at 750 and 850 °C showed a moderately higher ductility (increase in  $\epsilon_f\%$  of about 10%, Table 4), due to the subtraction of interstitial atoms from solid solutions, after the precipitation of chromium carbides and nitrides at the grain boundaries (Figure 2). All other aged samples presented  $\epsilon_f\%$  values close to that of the as-received one. As an example, Figure 10a shows the behaviour of the as-received sample and the samples aged at 850 °C for different times. A similar behaviour was observed on the alloy LDSS 2101, with a nitrogen content of 0.22 wt%, where an increment in ductility of about 40% after 30 min aging at 850 °C was detected, essentially due to a large chromium nitride precipitation [28]. In DSS 2304, the observed formation of ductile  $\gamma_2$  phase under prolonged aging could also have contributed to the  $\epsilon_f\%$  increase [43].

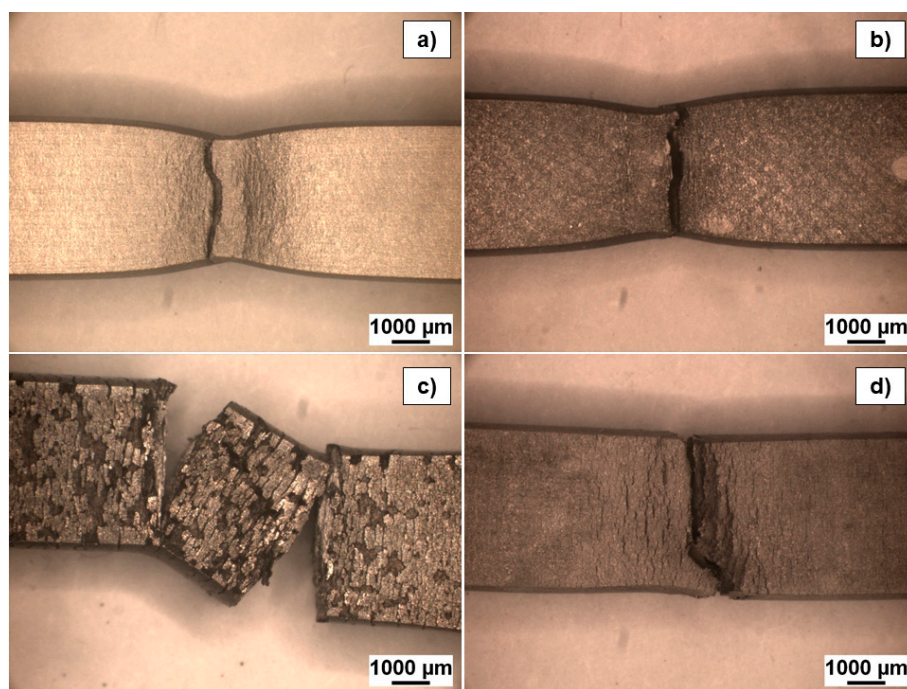


**Figure 10.** Stress—strain curves obtained with SSRT performed in air at 25 °C (a) and in NACE TM-0177 in the presence of  $10^{-3}$  M  $S_2O_3^{2-}$  (b) on DSS 2304, both as-received and aged at 850 °C for 5, 10 and 60 min.

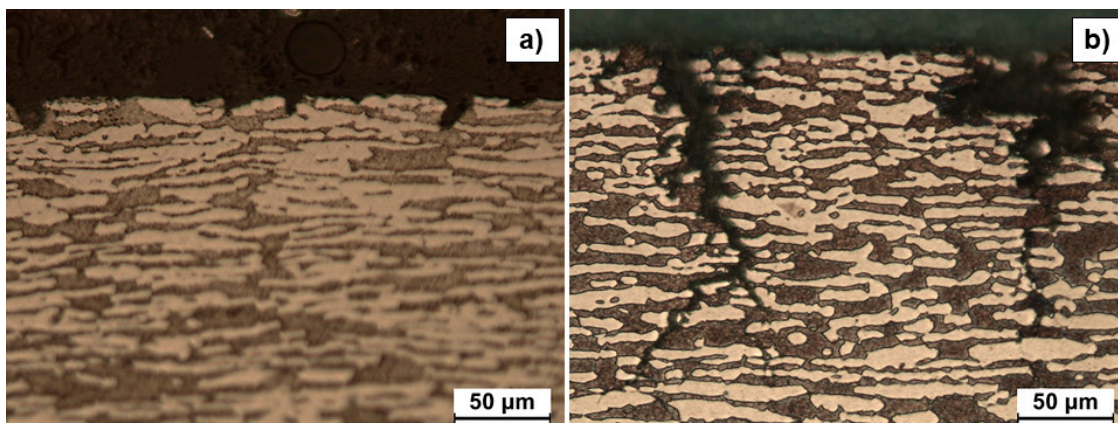
In NACE TM-0177 containing  $10^{-3}$  M  $S_2O_3^{2-}$ , all samples aged for 5 min maintained the same ductility as the as-received sample. On the contrary, at increasing aging time and temperature, a general reduction in  $\epsilon_f\%$  was observed, while only the sample aged for 60 min at 850 °C exhibited a partial recovery in SCC resistance (Table 4). In fact, as highlighted in Figure 10b, the sample aged for 5 min at 850 °C maintained its ductility, an aging of 10 min at 850 °C determined a relevant decrease in  $\epsilon_f\%$  from 53 to 22% and a recovery of ductility was observed by extending the aging time up to 60 min ( $\epsilon_f\% = 39\%$ ).

Figure 11 compares the extent of necking and the surface aspect of both the as-received sample (Figure 11a) and the samples aged at 850 °C (Figure 11b–d), at the end of SSRT. The as-received sample and that aged for 5 min showed a ductile-type fracture and a light general corrosion attack only on the latter. A brittle-type fracture occurred in DSS 2304 aged 10 min at 850 °C (Figure 11c), with evidence of numerous secondary cracks and presence of areas in which the corrosion attack became strongly localized (dark stains). For the sample aged at 850 °C, for the longest time (Figure 11d), the fracture was still of brittle-type, with presence of secondary crack propagation, but again a more generalized corrosion attack, instead of a localized one, was visible. The samples aged for 10 and 60 min at 750 °C and that aged for 60 min at 650 °C (not shown) presented a fracture morphology and a surface attack similar to the severe one exhibited in Figure 11c. Instead, DSS 2304 aged for only 10 min at 650 °C (not shown) behaved similarly to that aged 60 min at 850 °C. The behaviour of the other samples was similar to that of the as-received one.

The morphology of the corrosion attack observed in section on samples aged at 850 °C is shown in Figure 12. The sample in Figure 11b, aged for 5 min, clearly evidences the formation of several small pits which did not initiate cracks (Figure 12a). Differently, the sections of the sample in Figure 11c, aged for 10 min (Figure 12b), and that in Figure 11d, aged for 60 min (picture not reported), show that pits triggered many cracks, indicating SCC failure. These cracks mainly propagated in the ferrite phase or followed austenite/ferrite interface.



**Figure 11.** Macrograph acquired on the gauge length of DSS 2304 as-received (a) and aged at 850 °C for 5 (b), 10 (c) and 60 min (d) after SSRT in NACE TM-0177 in the presence of  $10^{-3}$  M  $\text{S}_2\text{O}_3^{2-}$ .



**Figure 12.** Micrographs of DSS 2304 aged for 5 (a) and 10 min (b) at 850 °C after SSRT in NACE solution containing  $10^{-3}$  M  $\text{S}_2\text{O}_3^{2-}$  (long transverse sections, parallel to load direction).

These differences may be rationalized by comparing the different potential trends shown during SSRT by the as-received sample and by the samples aged at 850 °C for different times (Figure 13). The  $E_{\text{OCP}}$  values of the as-received sample remained rather noble (around  $-0.25$  V<sub>SCE</sub>) throughout the test, indicating passive conditions [27,44], as confirmed by the visual aspect of the sample at the end of the exposure (Figure 11a). A significant initial  $E_{\text{OCP}}$  drop towards negative values was detected for DSS 2304 aged for 5 min at 850 °C. However, after a strain of about 6%, the sample recovered a passive state. Conversely, the  $E_{\text{OCP}}$  values of the sample aged for 10 min at 850 °C decreased rapidly and reached values close to  $-0.55$  V<sub>SCE</sub>. The same  $E_{\text{OCP}}$  trend was shown by the other samples showing significant ductility reduction (aging for 60 min at 650 and for 10 and 60 min at 750 °C). The sample aged for 60 min at 850 °C, characterized by a moderate ductility decrease, reached quite negative  $E_{\text{OCP}}$  values of about  $-0.5$  V<sub>SCE</sub>, but at a much slower rate. This also occurred for the sample aged at 650 °C for 10 min, exhibiting comparable ductility behaviour.

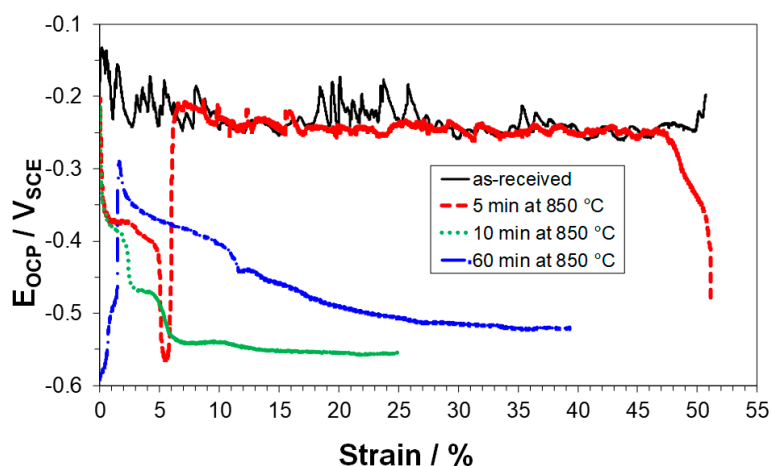


**Figure 13.**  $E_{OCP}$ —strain curves obtained with SSRT performed in NACE TM-0177 in the presence of  $10^{-3}$  M  $S_2O_3^{2-}$  on DSS 2304, both as-received and aged at 850 °C for 5, 10 and 60 min.

The potential-pH diagrams calculated for elementary sulphur and oxygen adsorbed on metals, such as Fe, Ni or Cr, and those calculated for the S-Fe (or Ni or Cr)-water systems at low S molality ( $10^{-4}$  mole/kg), at the temperature of 25 °C [44–46], suggest that at pH 2.7 all these  $E_{OCP}$  values in the range  $-0.25/-0.55$  V<sub>SCE</sub> are compatible with  $S_2O_3^{2-}$  ion reduction to adsorbed sulphur and  $H_2S$ . The amounts of these reduced species, capable of impairing the alloy passivity and favouring hydrogen penetration in the alloy, reasonably increased at decreasing  $E_{OCP}$  values, thus justifying the higher SCC susceptibility the longer the time persistence at quite negative  $E_{OCP}$  values.

The histogram reported in Figure 14 collects the R values obtained from SSRT results. The as-received sample and those aged for 5 min at the three different temperatures were not susceptible to SCC in the presence of  $S_2O_3^{2-}$ , as their R values were close to 1. By prolonging the aging time up to 10 min, the alloy became moderately susceptible to SCC already at 650 °C and much more susceptible at 750 and 850 °C. With an aging time of 60 min, the susceptibility was high at 650 °C and gradually decreased by raising the treatment temperature, showing a restoring of SCC resistance at 850 °C, as previously observed for  $E_{pitt}$  and CPT results.

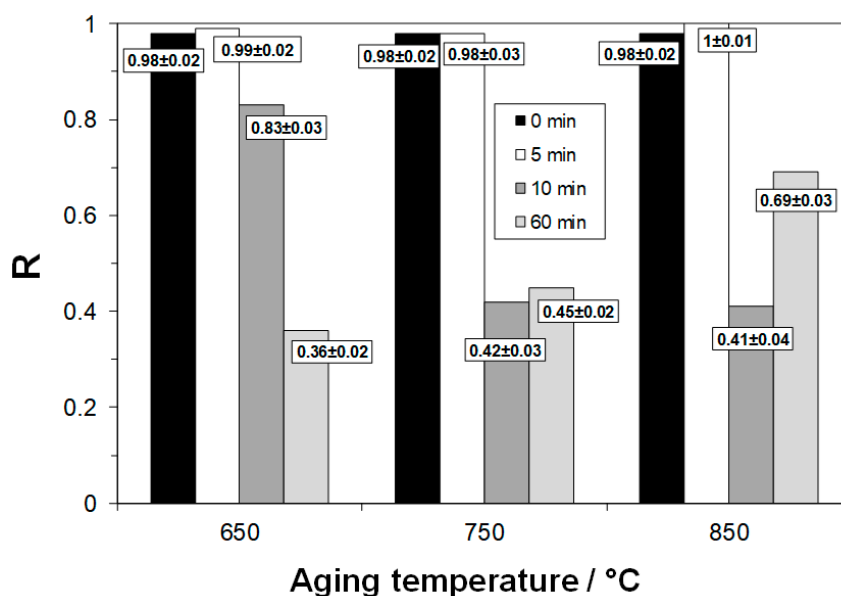


**Figure 14.** SCC susceptibility (R index) of DSS 2304, before and after thermal aging, obtained by SSRT in NACE solution containing  $10^{-3}$  M  $S_2O_3^{2-}$ .

#### 4. Discussion

This research shows that, in agreement with the literature [2,5,10], aging DSS 2304 samples between 650 and 850 °C induces the precipitation of chromium and molybdenum carbides (Figure 2), and perhaps nitrides (Figure 9). The nucleation of these precipitates occurs essentially at the  $\alpha/\gamma$  interface, acting as a connection between Cr-rich ferrite (which is also relatively rich in Mo) and C-rich austenite [10,47,48]. Then, carbides grow into the ferrite phase, because of the higher diffusivity of Cr and Mo in this phase [49]. As a consequence of carbide precipitation, conversion of ferrite phase close to carbides into  $\gamma_2$  phase (having a lower Cr and Mo content in comparison to  $\gamma$ ) occurs to a certain extent (Figure 2), because of ferrite instability after depletion in ferrite-stabilizing elements [4,40].  $\gamma_2$  phase and, likely, the narrow zone close to carbides in the original  $\gamma$  phase (depleted in passivating elements, like  $\gamma_2$ ) become the preferential sites for localized corrosion and IGC attack (Figures 6 and 9).

The 60 min treatments at 650 and 750 °C are the most critical for pitting corrosion resistance and IGC susceptibility, as they significantly worsen the alloy behaviour against these corrosion forms. The thermal aging at 850 °C did not affect IGC sensitization, but produced a moderate worsening in pitting resistance already after 5 min of permanence, which persisted after 10 min. A recovery of localized corrosion resistance was observed after the longest aging time, likely due to the high-temperature rediffusion of the key passivating alloying elements (Cr, Mo, N) from the phase cores towards the phase boundaries [11,15,50,51]. In agreement with the findings of other authors [1,52,53], at low aging temperatures (i.e., 650 and 750 °C) the precipitated carbides were small and finely distributed, while at 850 °C more discontinuous larger precipitates were detected as a consequence of the higher diffusion rates (Figure 1). Thus, the higher sensitization to localized corrosion attack obtained after long aging treatments at the two lower temperatures could also be due to the higher width and continuity of the Cr- and Mo-depleted areas.

The SSRT results on SCC susceptibility of as-received and thermally aged DSS 2304 in NACE solution containing  $10^{-3}$  M  $S_2O_3^{2-}$  are in good general agreement with pitting corrosion and IGC resistance. In particular, the conditions determining the best alloy behaviour towards pitting and IGC corrosion (as-received, 5 min at 650 °C and 5 min at 750 °C) are also quite resistant to SCC. Moreover, the aging conditions determining the lowest pitting resistance and highest sensitization to IGC (at 650 °C for 60 min and at 750 °C for 10 and 60 min) also induce the highest susceptibility to SCC in DSS 2304. In fact, the synergistic effect of  $Cl^-$  and  $S_2O_3^{2-}$  [54] leads to a much easier pit development in the areas depleted in passivating elements and finally to an earlier SCC failure, due to crack growth at the bottom of pits.

During the elastic deformation step in SSRT, the most SCC susceptible samples quickly reached quite negative  $E_{OCP}$  values of about  $-0.55 V_{SCE}$ , which were maintained for long times. Under these potential/pH conditions, a significant conversion of  $S_2O_3^{2-}$  into adsorbed sulphur and  $H_2S$  is expected [55], suggesting that, beside an active path mechanism, hydrogen penetration may also contribute to SCC failure [29,45]. As for pitting corrosion and IGC, also in the case of SCC, a long aging at 850 °C determines a recovery of DSS 2304 performance, most likely due to Cr- and Mo-rediffusion and to the formation of less continuous Cr- and Mo-depleted areas.

Some discrepancies among the relative resistance to different forms of localized corrosion refer to specimens subjected to thermal aging of intermediate severity. The differences detected can be ascribed to the different nature of the localized corrosion forms addressed and to the different conditions applied during the tests. As an example, both specimens aged for 5 and 10 min at 850 °C show some tendency to pitting corrosion in neutral chloride solution, due the presence of Cr- and Mo-depleted regions, even if the DOS values to IGC are low ( $I_r/I_a\% < 1$ ). It is likely that the impoverished areas are relatively narrow and discontinuous at this high aging temperature thus determining a limited IGC attack. The susceptibility to SCC of these same specimens is certainly influenced by the presence of regions depleted in passivating elements but, during the dynamic conditions applied by SSRT, cracks only develop if the metal repassivation rate decreases and becomes at least comparable to the rate of formation of new bare metal surfaces at the pit bottom. This is likely to occur in the case of the

10-min aged specimens that show a low R value. Instead, in the case of the 5-min aged specimens the repassivation rate likely remains too high for severe crack development and R values of about 1 are obtained.

## 5. Conclusions

1. The heat treatment in the 650–850 °C range on DSS 2304 determined the formation of chromium carbides at  $\alpha/\gamma$  interphase and, under some conditions, the growth of Cr- and Mo-depleted  $\gamma_2$  phase.
2. These microstructural modifications affected the localized corrosion performances of this alloy. Pitting and IGC mainly initiated in Cr- and Mo-depleted regions near to precipitates inside the  $\gamma_2$  and likely also the  $\gamma$  phases, then propagated in the ferrite matrix.
3.  $E_{\text{pitt}}$  and CPT values indicated a decrease in pitting resistance of DSS 2304 after 10 min aging at 650 and 750 °C, and the pitting behaviour worsened after longer aging time at these temperatures. At 850 °C, a 5-min aging was sufficient to markedly decrease the pitting resistance, but a recovery was observed after 60 min of aging.
4. Similarly, DL-EPR results evidenced a significant IGC sensitization of DSS 2304 after 10 min at 750 °C and 60-min aging at both 650 and 750 °C but no aging treatment at 850 °C was detrimental to the alloy IGC resistance.
5. As for pitting corrosion, SCC susceptibility in NACE solution containing  $10^{-3}$  M  $\text{S}_2\text{O}_3^{2-}$  was also detected after 10 min aging at 650 and 750 °C and increased after longer aging time. SCC also occurred on the sample aged for 10 min at 850 °C. A longer heat treatment at this high temperature ensured a recovery of SCC resistance.
6. SCC failure initiated at the bottom of pits and was likely stimulated by hydrogen penetration.

**Author Contributions:** F.Z. and C.M. designed and planned the experiments; F.Z. and V.G. carried out all the tests; F.Z. and Andrea Balbo examined the obtained data; F.Z., C.M. and Andrea Balbo wrote the paper.

**Funding:** This research received no external funding.

**Acknowledgments:** The authors wish to thank Mattia Merlin for heat treatments of the studied materials and Marco Frigo (Customer Service Manager of Outokumpu S.p.A.) for supplying DSS 2304 samples.

**Conflicts of Interest:** The authors declare no conflict of interest.

## References

1. Pohl, M.; Storz, O.; Glogowski, T. Effect of intermetallic precipitations on the properties of duplex stainless steel. *Mat. Charact.* **2007**, *58*, 65–71. [[CrossRef](#)]
2. Badji, R.; Kherrouba, N.; Mehdi, B.; Cheniti, B.; Bouabdallah, M.; Kahloun, C.; Bacroix, B. Precipitation kinetics and mechanical behavior in a solution treated and aged dual phase stainless steel. *Mater. Chem. Phys.* **2014**, *148*, 664–672. [[CrossRef](#)]
3. Wang Chan, K.; Chin Tjong, S. Effect of secondary phase precipitation on the corrosion behavior of Duplex Stainless Steels. *Materials* **2014**, *7*, 5268–5304. [[CrossRef](#)] [[PubMed](#)]
4. Escriba, D.M.; Materna-Morris, E.; Plaut, R.L.; Padilha, A.F. Chi-phase precipitation in a duplex stainless steel. *Mater. Charact.* **2009**, *60*, 1214–1219. [[CrossRef](#)]
5. Knyazeva, M.; Pohl, M. Duplex Steels. Part II: Carbides and Nitrides. *Metallogr. Microstruct. Anal.* **2013**, *2*, 343–351. [[CrossRef](#)]
6. Moura, V.S.; Lima, L.D.; Pardal, J.M.; Kina, A.Y.; Corte, R.R.A.; Tavares, S.S.M. Influence of microstructure on the corrosion resistance of the duplex stainless steel UNS S31803. *Mat. Charact.* **2008**, *59*, 1127–1132. [[CrossRef](#)]
7. Lopez, N.; Cid, M.; Puigalli, M. Influence of  $\sigma$ -phase on mechanical properties and corrosion resistance of duplex stainless steels. *Corros. Sci.* **1999**, *41*, 1615–1631. [[CrossRef](#)]

8. Lopez, N.; Cid, M.; Puigalli, M.; Azkarate, I.; Pelayo, A. Application of double loop electrochemical potentiodynamic reactivation test to austenitic and duplex stainless steels. *Mater. Sci. Eng. A* **1997**, *A229*, 123–128. [[CrossRef](#)]
9. Chen, T.H.; Yang, J.R. Effect of solution treatment and continuous cooling on  $\sigma$ -phase precipitation in a 2205 duplex stainless steel. *Mater. Sci. Eng. A* **2001**, *A311*, 28–41. [[CrossRef](#)]
10. Kashiwar, A.; Phani Vennela, N.; Kamath, S.L.; Khatirkar, R.K. Effect of solution annealing temperature on precipitation in 2205 duplex stainless steel. *Mat. Charact.* **2012**, *74*, 55–63. [[CrossRef](#)]
11. Sathirachinda, N.; Petterson, R.; Wessman, S.; Pan, J. Study of nobility of chromium nitrides in isothermally aged duplex stainless steels by using SKPFM and SEM/EDS. *Corros. Sci.* **2010**, *52*, 179–186. [[CrossRef](#)]
12. Zhang, L.; Jiang, Y.; Deng, B.; Zhang, W.; Xu, J.; Li, J. Effect of aging on the corrosion of 2101 lean duplex stainless steel. *Mat. Charact.* **2009**, *60*, 1522–1528. [[CrossRef](#)]
13. Ramirez, A.J.; Lippold, J.C.; Brandi, S.D. The relationship between Chromium Nitride and Secondary Austenite precipitation in Duplex Stainless Steels. *Metallurg. Mater. Trans. A* **2003**, *34A*, 1575–1596. [[CrossRef](#)]
14. Charles, J.; Chemelle, P. The history of duplex developments, nowadays DSS properties and duplex market future trends. In Proceedings of the 8th Duplex Stainless Steels Conference, Beaune, France, 13–15 October 2010.
15. Zanotto, F.; Grassi, V.; Merlin, M.; Balbo, A.; Zucchi, F. Effect of brief heat treatments performed between 650 and 850 °C on corrosion behaviour of a lean duplex stainless steel. *Corros. Sci.* **2015**, *94*, 38–47. [[CrossRef](#)]
16. Berner, M.; Liu, H.P.; Olsson, C.O.A. Estimating localized corrosion resistance of low alloy stainless steels: comparison of pitting potentials and critical pitting temperatures measured on lean duplex stainless steel LDX 2101 after sensitization. *Corros. Eng. Sci. Techn.* **2008**, *43*, 111–116. [[CrossRef](#)]
17. Liu, H.; Johansson, P.; Liljas, M. Structural evolution of LDX 2101® (EN 1.4162) during isothermal ageing at 600–850°C. In Proceedings of the 6th European Stainless Steel Conference, Science and Market, Helsinki, Finland, 10–13 June 2008; pp. 555–560.
18. Sun, K.; Zeng, M.; Shi, Y.; Hu, Y.; Shen, X. Microstructure and corrosion behavior of S32101 stainless steel underwater dry and wet welded joints. *J. Mater. Process. Tech.* **2018**, *256*, 190–201. [[CrossRef](#)]
19. Zhang, Z.; Zhao, H.; Zhang, H.; Yu, Z.; Hu, J.; He, L.; Li, J. Effect of isothermal aging on the pitting corrosion resistance of UNS S82441 duplex stainless steel based on electrochemical detection. *Corros. Sci.* **2015**, *93*, 120–125. [[CrossRef](#)]
20. Tan, H.; Wang, Z.; Jiang, Y.; Yang, Y.; Deng, B.; Song, H.; Li, J. Influence of welding thermal cycles on microstructure and pitting corrosion resistance of 2304 duplex stainless steels. *Corros. Sci.* **2012**, *55*, 368–377. [[CrossRef](#)]
21. Chen, L.; Tan, H.; Wang, Z.; Li, J.; Jiang, Y. Influence of cooling rate on microstructure evolution and pitting corrosion resistance in the simulated heat-affected zone of 2304 duplex stainless steels. *Corros. Sci.* **2012**, *58*, 168–174. [[CrossRef](#)]
22. Jiang, Y.; Tan, H.; Wang, Z.; Hong, J.; Jiang, L.; Li, J. Influence of Creq/Nieq on pitting corrosion resistance and mechanical properties of UNS S32304 duplex stainless steel welded joints. *Corros. Sci.* **2013**, *70*, 252–259. [[CrossRef](#)]
23. Pezzato, L.; Lago, M.; Brunelli, K.; Breda, M.; Piva, E.; Calliari, I. Effect of Secondary Phases Precipitation on Corrosion Resistance of Duplex Stainless Steels. *Mater. Sci. Forum* **2016**, *879*, 1495–1500. [[CrossRef](#)]
24. Guo, L.; Li, X.; Sun, T.; Xu, J.; Li, J.; Jiang, Y. The influence of sensitive temperature on the localized corrosion resistance of duplex stainless steel SAF2304. *Acta Metall. Sin.* **2012**, *48*, 1503–1509. [[CrossRef](#)]
25. Zhang, Z.; Han, D.; Jiang, Y.; Shi, C.; Li, J. Microstructural evolution and pitting resistance of annealed lean duplex stainless steel UNS S32304. *Nuclear Eng. Design* **2012**, *243*, 56–62. [[CrossRef](#)]
26. Zanotto, F.; Grassi, V.; Balbo, A.; Monticelli, C.; Zucchi, F. Stress corrosion cracking of LDX 2101® duplex stainless steel in chloride solutions in the presence of thiosulphate. *Corros. Sci.* **2014**, *80*, 205–212. [[CrossRef](#)]
27. Zanotto, F.; Grassi, V.; Balbo, A.; Monticelli, C.; Zucchi, F. Stress-Corrosion Cracking Behaviour of Lean-Duplex Stainless Steels in Chloride/Thiosulphate Environments. *Metals* **2018**, *8*, 237. [[CrossRef](#)]
28. Zanotto, F.; Grassi, V.; Balbo, A.; Monticelli, C.; Melandri, C.; Zucchi, F. Effect of brief thermal aging on stress corrosion cracking susceptibility of LDSS 2101 in the presence of chloride and thiosulphate ions. *Corros. Sci.* **2018**, *130*, 22–30. [[CrossRef](#)]

29. Tsujikawa, S.; Miyasaka, A.; Ueda, M.; Ando, S.; Shibata, T.; Haruna, T.; Katahira, M.; Yamane, Y.; Aoki, T.; Yamada, T. Alternative for evaluating sour gas resistance of low-alloy steels and corrosion-resistant alloys. *Corrosion* **1993**, *49*, 409–419. [[CrossRef](#)]
30. He, L.; Guo, Y.-J.; Wu, X.-Y.; Jiang, Y.-M.; Li, J. Effect of Solution Annealing Temperature on Pitting Behavior of Duplex Stainless Steel 2204 in Chloride Solutions. *J. Iron Steel Res. Int.* **2016**, *23*, 357–363. [[CrossRef](#)]
31. International Organization for Standardization. *UNI EN ISO 17864:2005: Corrosion of Metals and Alloys—Determination of the Critical Pitting Temperature under Potentiostatic Control*; International Organization for Standardization: Geneva, Switzerland, 2005.
32. ASTM International. *ASTM A262 Standard Practices for Detecting Susceptibility to Intergranular Attack in Austenitic Stainless Steel*; ASTM International: West Conshohocken, PA, USA, 2015.
33. International Organization for Standardization. *ISO 12732:2006 Corrosion of Metals and Alloys—Electrochemical Potentiokinetic Reactivation Measurement Using the Double Loop Method (Based on Cihal's Method)*; International Organization for Standardization: Geneva, Switzerland, 2006.
34. Hong, J.; Han, D.; Tan, H.; Li, J.; Jiang, Y. Evaluation of aged duplex stainless steel UNS S32750 susceptibility to intergranular corrosion by optimized double loop electrochemical potentiokinetic reactivation method. *Corros. Sci.* **2013**, *68*, 249–255. [[CrossRef](#)]
35. Wasnik, D.N.; Kain, V.; Samajdar, I.; Verlinden, B.; De, P.K. Resistance to sensitization and intergranular corrosion through extreme randomization of grain boundaries. *Acta Mater.* **2002**, *50*, 4587–4601. [[CrossRef](#)]
36. *NACE standard TM-0177-90 Standard Test Method Laboratory Testing of Metals for Resistance to Sulfide Stress Cracking in H2S Environments*; NACE International: Huston, TX, USA, 1990.
37. Barteri, M.; De Cristofaro, N.; Scoppio, L.; Cumino, G.; Della Pina, G. Corrosion resistance of martensitic stainless steels in moderately sour oilfield environments. In Proceedings of the Corrosion '95, NACE, Houston, TX, USA, 26–31 March 1995; p. 76.
38. Garzon, C.M.; Ramirez, A.J. Growth kinetics of secondary austenite in the welding microstructure of a UNS S32304 duplex stainless steel. *Acta Mater.* **2006**, *54*, 3321–3331. [[CrossRef](#)]
39. Calliari, I.; Pellizzari, M.; Baldo, S.; Zanellato, M.; Ramous, E. Analysis of phase stability in Cr-Ni and Cr-Mn DSS. In Proceedings of the 8th Duplex Stainless Steels Conference, Beaune, France, 10–13 June 2008.
40. Maetz, J.-Y.; Douillard, T.; Cazottes, S.; Verdu, C.; Kléber, X.  $M_{23}C_6$  carbides and  $Cr_2N$  nitrides in aged duplex stainless steel: A SEM, TEM and FIB tomography investigation. *Micron* **2016**, *84*, 43–53. [[CrossRef](#)]
41. Gong, J.; Jiang, Y.M.; Deng, B.; Xu, J.L.; Hu, J.P.; Li, J. Evaluation of intergranular corrosion susceptibility of UNS S31803 duplex stainless steel with an optimized double loop electrochemical potentiokinetic reactivation method. *Electrochem. Acta* **2010**, *55*, 5077–5083. [[CrossRef](#)]
42. Amadou, T.; Braham, C.; Sidhom, H. Double Loop Electrochemical Potentiokinetic Reactivation Test Optimization in Checking of Duplex Stainless Steel Intergranular Corrosion Susceptibility. *Metall. Mater. Trans. A* **2004**, *35A*, 3499–3513. [[CrossRef](#)]
43. Fang, Y.L.; Liu, Z.Y.; Xue, W.Y.; Song, H.M.; Jiang, L.Z. Precipitation of secondary phases in lean duplex stainless steel 2101 during isothermal ageing. *ISIJ Int.* **2010**, *50*, 286–293. [[CrossRef](#)]
44. Marcus, P.; Oudar, J. *Corrosion Mechanism in Theory and Practice*, 2nd ed.; Marcel Dekker Inc.: New York, NY, USA, 1995; pp. 240–248. ISBN 0-8247-0666-8.
45. Choudhary, L.; Macdonald, D.D.; Alfantazi, A.A. Role of thiosulfate in the corrosion of steels: A review. *Corrosion* **2015**, *71*, 1147–1168. [[CrossRef](#)]
46. Marcus, P.; Protopopoff, E. Thermodynamics of thiosulphate reduction on surfaces of iron, nickel and chromium in water at 25 and 300 °C. *Corros. Sci.* **1997**, *39*, 1741–1752. [[CrossRef](#)]
47. Lee, K.M.; Cho, H.S.; Choi, D.C. Effect of isothermal treatment of SAF 2205 duplex stainless steel on migration of interface boundary and growth of austenite. *J. Comp.* **1999**, *285*, 156–161. [[CrossRef](#)]
48. Cheng, X.; Wang, Y.; Lia, X.; Dong, C. Interaction between austenite-ferrite phases on passive performance of 2205 duplex stainless steel. *J. Mater. Sci. Technol.* **2018**, *34*, 2140–2148. [[CrossRef](#)]
49. Devine, T.M. Kinetics of Sensitization and De-Sensitization on Duplex 308 Stainless Steel. *Acta Metall.* **1988**, *36*, 1491–1501. [[CrossRef](#)]
50. Aydoğdu, G.H.; Aydinol, M.K. Determination of susceptibility to intergranular corrosion and electrochemical reactivation behaviour of AISI 316L type stainless steel. *Corros. Sci.* **2006**, *48*, 3565–3583.
51. Mehrer, H. *Diffusion in Solids Fundamentals, Methods, Materials, Diffusion-Controlled Processes*; Springer: Berlin, Germany, 2007; pp. 127–130.

52. Deng, B.; Jiang, Y.; Gong, J.; Zhong, C.; Gao, J.; Li, J. Critical pitting and repassivation temperatures for duplex stainless steel in chloride solutions. *Electrochim. Acta* **2008**, *53*, 5220–5225. [[CrossRef](#)]
53. Bettini, E.; Kivisäkk, U.; Leygraf, C.; Pan, J. Study of corrosion behavior of a 22% Cr duplex stainless steel: Influence of nano-sized chromium nitrides and exposure temperature. *Electrochim. Acta* **2013**, *113*, 280–289. [[CrossRef](#)]
54. Newman, R.C.; Isaacs, H.S.; Alman, B. Effect of sulfur compounds on the pitting behavior of type 304 stainless steel in near-neutral chloride solutions. *Corrosion* **1982**, *38*, 261–264. [[CrossRef](#)]
55. Rhodes, P.R.; Welch, G.A.; Abrego, L. Stress corrosion cracking susceptibility of duplex stainless steels in sour gas environments. *J. Mater. Energy Syst.* **1983**, *5*, 3–18. [[CrossRef](#)]



© 2018 by the authors. Licensee MDPI, Basel, Switzerland. This article is an open access article distributed under the terms and conditions of the Creative Commons Attribution (CC BY) license (<http://creativecommons.org/licenses/by/4.0/>).